JOURNAL OF AIRCRAFT
Vol. 30, No. 6, Nov.–Dec. 1993

Analytical-Experimental Investigation of Free-Vibration Characteristics of Rotating Composite I-Beams

Ramesh Chandra* and Inderjit Chopra†
University of Maryland, College Park, Maryland 20742

This article presents a free-vibration analysis of coupled composite I-beams with couplings under rotation. A linear analysis based upon Vlasov theory was developed to obtain coupled flap-lag-torsion equations of motion for I-beams made out of general composite laminates. Constrained warping and transverse shear effects were included. Free-vibration characteristics were obtained by solving these equations using Galerkin's method. In order to validate the theory, graphite-epoxy and kevlar-epoxy I-beams with bending-torsion coupling were fabricated using an autoclave molding technique and tested in an in vacuo rotor test facility for their vibration characteristics. Induced-strain actuation by piezoceramic elements was used to excite the I-beams in the rotating frame. Strain gauges were used to measure the response of these beams over a range of rotational speeds up to 1000 rpm. Natural frequencies and strain mode shapes were determined by carrying out signal analysis using a spectrum analyzer. Good correlation between theory and experiment was achieved. About 600% increase in torsional frequency due to constrained warping occurs for graphite-epoxy beams with a slenderness ratio of 18.

Nomenclature

A = cross-sectional area of blade
b, h = semiwidth and semiheight of I-beam
E_l, E_t = Young's moduli in principal directions of plies of beam
G_{lt} = shear modulus of plies in principal plane
I_{xx}, I_{yy} = blade cross-sectional moment of inertia about x and y axes, respectively
$[K]$ = stiffness matrix for beam
$[K_f]$ = flap bending stiffness matrix
$[K_{ft}]$ = flap bending-torsion coupling stiffness matrix
$[K_l]$ = lag bending stiffness matrix
$[K_{lt}]$ = lag bending-torsion coupling stiffness matrix
$[K_t]$ = torsion stiffness matrix
K_A = effective polar radius of gyration of blade cross-section $\sqrt{(I_{yy} + I_{xx})/A}$
K_m = $\sqrt{K_{m1}^2 + K_{m2}^2}$
K_{m1}, K_{m2} = principal mass radii of gyration of beam cross section
M_x, M_y = bending moments
M_ω = bimoment (or warping moment)
m = mass per unit length of blade
N = axial force
p_x, p_y, p_z = inertial forces
q_x, q_y, q_z = inertial moments
r = length of I-beam
s, z, n = coordinate system for plate segment of I-beam, Fig. 1a
T = torsion moment
t = time
U, V, W = displacements in x, y, z directions
V_x, V_y = shear forces in x, y directions
x, y, z = coordinate system for I-beam, Fig. 1a
$\varepsilon_{xz}, \varepsilon_{yz}$ = transverse shear strains for the beam in xz and yz planes, respectively
μ = constrained warping parameter
μ_{lt} = major Poisson's ratio of plies in principal plane; first subscript denotes load direction, second refers to lateral direction
ϕ_x, ϕ_y, ϕ_z = rotations about x, y, z axes
Ω = rotational speed, rad/s

Superscripts
T = transpose
$( )'$ = differentiation with respect to z coordinate of beam

Introduction

WITH the application of high-performance composite materials, the design feasibility of advanced rotor systems such as hingeless and bearingless rotors is becoming a reality. Superior fatigue characteristics and flexibility to tailor structural characteristics are the key factors for the growing application of composites in the rotorcraft industry. Due to the lack of validated composite analytical models, an extreme level of conservatism is used in rotorcraft design. Also, the potential benefits of structural couplings due to composites are not explored at this time. Analyses of composite beam structures are more involved because nonclassical phenomena such as section warping, transverse shear, and warping constraint become significant. For the full exploration of composites to improve the performance of current helicopters and also to meet many challenging missions of future helicopters, it is necessary to develop and validate analyses of composite blades.

Thin-walled composite beams with closed and open cross sections are widely used in the construction of rotor blades. Recently, there have been a growing number of research activities to model behavior of thin-walled composite beams, ranging from simple analytical models[1–4] to detailed finite element models.[5–7] There have also been some selected validations for these models for static and vibration characteristics[8–13] and a few investigations to examine the aeroelastic behavior of composite rotors.[14–16] These studies showed that the structural couplings due to composites can be used to reduce vibration and blade bending stresses and improve aeromechanical stability.

Stringent design requirements for flex-beams, a key component of bearingless rotors,[17] can be met by building them as open-section composite beams. However, most of the available literature on thin-walled composite beams[1–16] is focused on closed-section beams (box-beams). The objective of this

Received Dec. 12, 1991; revision received Aug. 20, 1992; accepted for publication Sept. 11, 1992.

*Assistant Research Scientist, Department of Aerospace Engineering. Member AIAA.
†Professor, Department of Aerospace Engineering. Fellow AIAA.

article is to formulate a dynamic analysis of thin-walled open-section composite beams and then validate the analysis by correlating the calculated frequencies and mode shapes of several composite I-beams with measured values under rotating and nonrotating environments.

Hong and Chopra[16] presented an aeroelastic stability analysis of a composite bearingless rotor blade. In that study, the flexbeam was an open-section composite beam (I-beam) and outboard main blade and torque tube were made out of isotropic materials. The flanges and web of the I-beam were designed to give bending-torsion (for symmetric I-beams) and extension-torsion (for antisymmetric I-beams) couplings. Very significant influence of these elastic couplings on blade dynamics was shown. The structural model used was based on the solid section approach; constrained warping and transverse shear effects were not included.

Rehfield and Atilgan[18] presented a buckling analysis of composite open-section beams. The wall thickness of the beam was assumed to be thin enough to neglect its bending stiffness, but the transverse shear deformations of the beam cross section was included.

Vlasov[19] and Gjelsvik[20] presented an isotropic beam theory for open and closed sections. In that theory, two-dimensional stress and displacement fields of beams were identified with those of plate/shell segments of the beam. The generalized beam displacements were obtained from plate/shell displacements through geometric considerations, whereas the generalized beam forces and their equilibrium equations were obtained using the principle of virtual work. Transverse shear deformation was not included. Bauld and Tzeng[21] extended Vlasov theory to open sections made out of composite materials. However, it was confined to sections where the flanges and webs were symmetric with respect to their own midsurfaces.

The authors[22] expanded Vlasov theory to open-section beams made out of general composite laminates. Thus, the restriction imposed by Bauld and Tzeng[21] on the lay-up of flanges and webs of beam was removed. Also, the transverse shear deformation was included. The analysis was systematically validated by experiments. Several graphite-epoxy and Kevlar®-epoxy I-beams with bending-torsion couplings covering different parameters were fabricated using an autoclave molding technique. These beams were tested for their structural response under bending and torsional loads. Good correlation between theory and experiment was achieved. Constrained warping and extension-twist coupling of the flanges were found to have significant influence on structural response of those beams.

In the present investigation, the free-vibration behavior of composite I-beams with elastic couplings under rotation is examined. Based on the structural model of Ref. 22, the governing differential equations for flap-lag-torsion motion of I-beams under the regime of linear theory were derived. These equations were solved using Galerkin's method to obtain natural frequencies and mode shapes. The experimental natural frequencies and mode shapes were obtained by testing the I-beams in an in vacuo rotor test facility. Induced-strain actuation by piezoceramic devices was used to excite the rotating beams in flap and torsion modes. Strain gauges were used to measure the response of the beams. Frequencies and mode shapes were determined by analyzing the strain gauge signals using a spectrum analyzer.

Analysis

In this article, a linear dynamic analysis is developed to predict the free-vibration characteristics of open-section composite beams under rotation. The nonclassical effects, like section warping and transverse shear-related couplings, are included. Flanges and webs of open-section beams are modeled as general composite laminates, and two-dimensional stress and displacement fields associated with these are reduced to one-dimensional generalized beam forces and displacements. The generalized beam displacements are connected to plate displacements through geometric considerations, whereas the generalized beam forces and their equilibrium equations are obtained using the principle of virtual work.

Kinematics

From geometric considerations, the displacements associated with any generic plate-segment of the beam are related to the beam displacements U, V, and ϕ_z as

$$u(z, s) = U(z)\sin\theta(s) - V(z)\cos\theta(s) - q(s)\phi_z(z) \quad (1)$$

$$v(z, s) = U(z)\cos\theta(s) + V(z)\sin\theta(s) + r(s)\phi_z(z) \quad (2)$$

where r, q, and θ are defined in Fig. 1b.

The axial displacement $w(z, s)$ is determined from the following shear strain-displacement relation:

$$\varepsilon_{zs} = w_{,s} + v_{,z} \quad (3)$$

Note that ε_{sz} in the absence of transverse shear deformation is zero[19,20] for open-section beams. However, in the presence of transverse shear deformation

$$\varepsilon_{zs} = \varepsilon_{xz}\cos\theta + \varepsilon_{yz}\sin\theta \quad (4)$$

Using Eqs. (3) and (4), $w(z, s)$ is obtained as

$$w(z, s) = W + x\phi_x + y\phi_y - \varphi\phi_z' \quad (5)$$

where φ is a warping function and is expressed in terms of sectorial area

$$\varphi = \int_s r\,ds$$

$$\phi_x = \varepsilon_{xz} - U' \quad (6)$$

$$\phi_y = \varepsilon_{yz} - V'$$

Note that the deformation of the beam is completely described by six generalized displacements: three translations

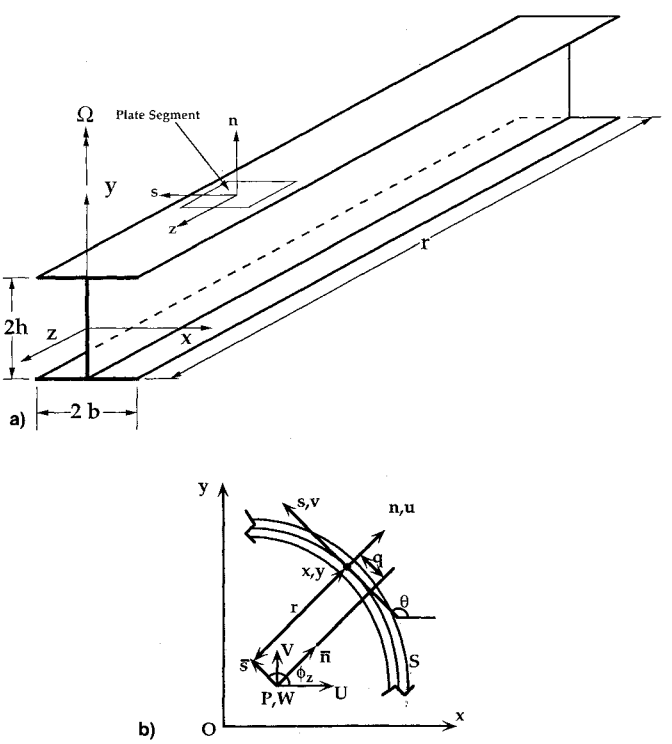

Fig. 1 a) Coordinates in I-beam and b) pictorial definitions of blade displacements and rotations.

(U, V, W) and three rotations (ϕ_x, ϕ_y, and ϕ_z). Also, the Eqs. (1), (2), and (5) connect these displacements to the plate displacements.

Using Eqs. (1), (2), and (5), strain-displacements relations, and constitutive relations for a general laminate, the stress and moment resultants associated with a generic plate segment of the beam are expressed in terms of the generalized beam displacements.

The generalized beam forces and their equilibrium equations are derived using the principle of virtual work. The generalized beam forces are N, V_x, V_y, M_x, M_y, T, and M_ω. These are obtained in terms of stress and moment resultants of the plate segment. It is important to note that the torsion corresponding to constrained warping is accounted for by M_ω, which is a bimoment. The total torsion T is considered as consisting of St. Venant torsion T_s (free-warping torsion) and Vlasov torsion T_ω (constrained warping torsion). The force-displacement relations for a bending-torsion coupled open-section beam[22] are as follows:

Extension-Transverse Shear

$$\begin{bmatrix} N \\ G_x \\ G_y \end{bmatrix} = \begin{bmatrix} K_{11} & K_{16} & K_{17} \\ K_{16} & K_{66} & 0 \\ K_{17} & 0 & K_{77} \end{bmatrix} \begin{bmatrix} W' \\ \varepsilon_{xz} \\ \varepsilon_{yz} \end{bmatrix} \tag{7}$$

Bending-Torsion

$$\begin{bmatrix} M_x \\ -M_y \\ M_\omega \\ T_s \\ F_x \\ F_y \end{bmatrix} = \begin{bmatrix} K_{22} & 0 & 0 & K_{25} & 0 & K_{29} \\ 0 & K_{33} & 0 & 0 & K_{38} & 0 \\ 0 & 0 & K_{44} & 0 & 0 & 0 \\ K_{25} & 0 & 0 & K_{55} & 0 & K_{59} \\ 0 & K_{38} & 0 & 0 & K_{88} & 0 \\ 0 & K_{29} & 0 & K_{59} & 0 & K_{99} \end{bmatrix} \begin{bmatrix} \phi'_y \\ \phi'_x \\ \phi''_z \\ \phi'_z \\ \varepsilon'_{xz} \\ \varepsilon'_{yz} \end{bmatrix} \tag{8}$$

where coefficients K_{ij} are defined in Ref. 22.

Following Ref. 22, the six governing equations can be written as

$$N' + p_z = 0 \tag{9}$$

$$M''_y - (NU')' - p_x = 0 \tag{10}$$

$$M''_x + (NV')' + p_y = 0 \tag{11}$$

$$M''_\omega - T'_s - q_z = 0 \tag{12}$$

$$F'_x - G_x = 0 \tag{13}$$

$$F'_y - G_y = 0 \tag{14}$$

where

$$\begin{aligned} p_x &= -m(U_{,tt} - \Omega^2 U); \qquad p_y = -mV_{,tt} \\ p_z &= m\Omega^2 z; \qquad q_x = 0; \qquad q_y = 0 \\ q_z &= mK_m^2\phi_{z,tt} + \tfrac{1}{2}m\Omega^2(K_{m2}^2 - K_{m1}^2)\sin 2\phi_z; \qquad m_\omega = 0 \end{aligned} \tag{15}$$

These inertia forces and moments are taken from Ref. 23.

These six equations along with the generalized force-displacement relations are used to obtain six governing equations in six generalized displacements, which are required to describe the dynamic behavior of these beams. Note that the transverse shear deformation in this analysis is represented by rotations (ϕ_x and ϕ_y). Vibration characteristics associated with bending, twisting, extension, and shear deformations of the beam can be obtained by solving the resulting six governing equations. However, this article is primarily concerned with the vibration characteristics of bending-torsion coupled beams associated with bending and twisting deformations. Hence, the three governing equations for flap, lag, and torsion are considered. Note that the frequencies associated with shear and extensional modes are expected to be high and are not considered; also, the extension-transverse shear coupling would influence the vibration characteristics associated with these modes.

Flap

$$m\frac{\partial^2 V}{\partial t^2} + K_{22}\frac{\partial^4 V}{\partial z^4} + K_{25}\frac{\partial^3 \phi_z}{\partial z^3} - \frac{1}{2}m\Omega^2\frac{\partial}{\partial z}\left[\frac{\partial V}{\partial z}(r^2 - z^2)\right] = 0 \tag{16}$$

Lag

$$m\frac{\partial^2 U}{\partial t^2} + K_{33}\frac{\partial^4 U}{\partial z^4} + K_{35}\frac{\partial^3 \phi_z}{\partial z^3} - m\Omega^2 U - \frac{1}{2}m\Omega^2\frac{\partial}{\partial z}\left[\frac{\partial U}{\partial z}(r^2 - z^2)\right] = 0 \tag{17}$$

Torsion

$$mK_m^2\frac{\partial^2 \phi_z}{\partial t^2} + K_{44}\frac{\partial^4 \phi_z}{\partial z^4} - K_{55}\frac{\partial^2 \phi_z}{\partial z^2} - K_{25}\frac{\partial^3 V}{\partial z^3} - K_{35}\frac{\partial^3 U}{\partial z^3} + m\Omega^2(K_{m2}^2 - K_{m1}^2)\phi_z - \frac{1}{2}m\Omega^2 K_A^2\frac{\partial}{\partial z}\left[\frac{\partial \phi_z}{\partial z}(r^2 - z^2)\right] = 0 \tag{18}$$

Method of Solution

The coupled differential equations are solved using Galerkin's method. The displacements U, V, and ϕ_z are assumed as

$$U = \sum_{i=1}^{n} b_i\psi_i \tag{19}$$

$$V = \sum_{i=1}^{n} a_i\psi_i \tag{20}$$

$$\phi_z = \sum_{i=1}^{n} c_i \sin\left(\frac{2i-1}{2}\frac{\pi z}{r}\right) \tag{21}$$

where ψ_i are beam functions.

For a cantilevered beam, the functions ψ_i are given

$$\psi_i = \cosh\frac{\lambda_i z}{r} - \cos\frac{\lambda_i z}{r} - \alpha_i\left(\sinh\frac{\lambda_i z}{r} - \sin\frac{\lambda_i z}{r}\right) \tag{22}$$

λ_i and α_i are coefficients given below:

i	1	2	3
λ_i	1.8751	4.6941	7.8548
α_i	0.7341	1.0185	0.9992

Note that the mode shapes described by Eqs. (19–21) correspond to a uniform cantilevered beam. The twist mode corresponds to the St. Venant torsion.

Applying Galerkin's method to Eqs. (16–18), the following coupled linear first-order differential equations are obtained:

$$\begin{aligned} m\{a\}_{,tt} + [K_f]\{a\} + [K_{ft}]\{c\} &= 0 \\ m\{b\}_{,tt} + [K_l]\{b\} + [K_{lt}]\{c\} &= 0 \\ mK_m^2\{c\}_{,tt} + [K_t]\{c\} + [K_{tf}]\{a\} + [K_{tl}]\{b\} &= 0 \end{aligned} \tag{23}$$

where

$$\{a\} = \{a_1, a_2, a_3, \ldots, a_n\}^T$$
$$\{b\} = \{b_1, b_2, b_3, \ldots, b_n\}^T \quad (24)$$
$$\{c\} = \{c_1, c_2, c_3, \ldots, c_n\}^T$$

$$[K_f] = \frac{K_{22}}{r^4}[P] - \frac{m\Omega^2}{2r}[I_2]^T + \frac{m\Omega^2}{r}[I_3]^T$$

$$[K_{ft}] = \frac{\pi^3}{8r^4}K_{25}[I_1]^T$$

$$[K_l] = \frac{K_{33}}{r^4}[P] - m\Omega^2[I] - \frac{m\Omega^2}{2r}[I_2]^T + \frac{m\Omega^2}{r}[I_3]^T$$

$$[K_{lt}] = \frac{\pi^3}{8r^4}K_{35}[I_1]^T$$

$$[K_t] = \frac{\pi^2}{4r^2}K_{55}[Q] - m\Omega^2(K_{m2}^2 - K_{m1}^2)[I] \quad (25)$$
$$+ \frac{\pi^2}{4}m\Omega^2\frac{K_A^2}{r^3}[I_5]^T - \frac{\pi^2}{4}m\Omega^2\frac{K_A^2}{r^3}[I_6]^T + \frac{\pi^4}{16}\frac{K_{44}}{r^4}[R]$$

$$[K_{tf}] = -\frac{2}{r}K_{25}[I_4]^T$$

$$[K_{tl}] = -\frac{2}{r}K_{35}[I_4]^T$$

$$[K_{55}]_r = K_{55} - K_{25}^2/K_{22}$$

$$\mu = l\sqrt{(K_{55})_r/K_{44}}$$

Matrices $[I_1]$–$[I_6]$, $[I]$, $[P]$, $[Q]$, and $[R]$ are defined in the Appendix.

Note that the natural frequencies of the rotating beams are mainly controlled by the stiffness matrices $[K_f]$, $[K_{ft}]$, $[K_l]$, $[K_{lt}]$, $[K_t]$, $[K_{tf}]$, and $[K_{tl}]$. These matrices in turn are influenced by K_{22}, K_{25}, K_{55}, K_{33}, K_{35}, and K_{44} stiffness coefficients of the force-displacement relations. It can be seen from the expression of $[K_t]$ that the constrained warping increases the torsional stiffness matrix via K_{44}. The Eqs. (23) are solved to calculate the natural frequencies and mode shapes. Three terms in Eqs. (19–21) are considered for these computations.

Experiments

In order to validate the present analysis, graphite-epoxy and Kevlar-epoxy I-beams with bending-torsion coupling were built by employing an autoclave molding technique. The details of the fabrication of beam specimens are given in Ref. 22. Composite prepreg layers were laid-up on a metal mold which consisted of two parts. Each of these parts would yield beams of C-section. For the fabrication of I-section beams, each part of the mold was wrapped with the desired number of prepreg layers. These layers were compacted by applying vacuum between the mold and lay-up. The two parts of the mold were placed back to back and additional layers in the flanges were introduced. Peel ply was wrapped to provide the surface finish of the beam. In order to bleed out excess resin and to permit the escape of volatiles during the curing process, a number of bleeder and breather layers were then applied. The lay-up was cured in a microprocessor-controlled autoclave as per the curing cycle given by the manufacturer. Thus, several graphite-epoxy and Kevlar-epoxy I-beams with a length of 36 in. were built. Note that the curing temperatures did not induce any warping deformation in these beams. Table 1 shows the details of these I-beams. The beams with the angle plies in the flanges have bending-torsion and extension-shear couplings.

These I-beams were tested for their free vibration characteristics in an in vacuo rotor test facility. The facility consists of a 10-ft-diam by 4-ft-high vacuum chamber, a rotary vane vacuum pump, a variable speed dc motor, and 100 channel slip-ring system. The rotational speed is sensed by a photo cell. The details of this facility are given in Ref. 9.

The excitation of rotating beams in the vacuum chamber was effected by means of piezoceramic devices via induced strain actuation. Note that the mechanical shakers are hard to use in the rotating frame. Lee[24] used an electromechanical shaker to excite the blades from outside the chamber, but did

Table 1 Details of thin-walled composite I-beams

Cases	Width and height, in.	Flanges: Top	Flanges: Bottom	Web	Length, in.	Clamped length, in.	Wall thickness, in.
Beams for experimental correlation[a]							
IB 1	1 × 1	$[0/90]_3/[15]_2$	$[0/90]_3/[-15]_2$	$[0/90]_4$	36	6.0	0.04
IB 2	1 × 0.5	$[0/90]_4$	$[0/90]_4$	$[0/90]_4$	36	2.5	0.04
IB 3	1 × 0.5	$[0/90]_3/[15]_2$	$[0/90]_3/[-15]_2$	$[0/90]_4$	36	2.5	0.04
IB 4	1 × 0.5	$[0/90]_3/[30]_2$	$[0/90]_3/[-30]_2$	$[0/90]_4$	36	2.5	0.04
IB 5	1 × 0.5	$[0/90]_3/[45]_2$	$[0/90]_3/[-45]_2$	$[0/90]_4$	36	2.5	0.04
Beams for experimental correlation[b]							
IB 6	1 × 0.5	$[0/90]_4$	$[0/90]_4$	$[0/90]_4$	36	2.5	0.072
IB 7	1 × 0.5	$[0/90]_3/[15]_2$	$[0/90]_3/[-15]_2$	$[0/90]_4$	36	2.5	0.072
IB 8	1 × 0.5	$[0/90]_3/[30]_2$	$[0/90]_3/[-30]_2$	$[0/90]_4$	36	2.5	0.072
IB 9	1 × 0.5	$[0/90]_3/[45]_2$	$[0/90]_3/[-45]_2$	$[0/90]_4$	36	2.5	0.072
Beams for numerical parametric study[c]							
IB 10	2 × 2	$[0/90]_2$	$[0/90]_2$	$[0/90]_2$	36	—	0.02
IB 11	1 × 0.5	$[0/90]_2$	$[0/90]_2$	$[0/90]_2$	36	—	0.02
IB 12	1 × 0.25	$[0/90]_2$	$[0/90]_2$	$[0/90]_2$	36	—	0.02
IB 13	1 × 0.25	$[0/90]/[15]_2$	$[0/90]/[-15]_2$	$[0/90]_2$	36	—	0.02

[a]Graphite-epoxy I-beam parameters: $E_l = 20.59 \times 10^6$ psi, $E_t = 1.42 \times 10^6$ psi, $G_{lt} = 0.89 \times 10^6$ psi, $\mu_{lt} = 0.42$, $G_{ln} = G_{tn} = 0.8 \times 10^6$ psi, $\mu_{ln} = 0.54$. Density $= 0.144 \times 10^{-3}$ lbs^2/in.^{4}. Ply thickness = 0.005 in.

[b]Kevlar-epoxy I-beam parameters: $E_l = 11 \times 10^6$ psi, $E_t = 0.8 \times 10^6$ psi, $G_{lt} = 0.34 \times 10^6$ psi, $\mu_{lt} = 0.34$, density $= 0.116 \times 10^{-3}$ lbs^2/in.^{4}. Ply thickness = 0.009 in.

[c]Graphite-epoxy I-beam parameters: $E_l = 20.59 \times 10^6$ psi, $E_t = 1.42 \times 10^6$ psi, $G_{lt} = 0.89 \times 10^6$ psi, $\mu_{lt} = 0.42$, $G_{ln} = G_{tn} = 0.8 \times 10^6$ psi, $\mu_{ln} = 0.54$. Density $= 0.144 \times 10^{-3}$ lbs^2/in.^{4}. Ply thickness = 0.005 in.

not succeed in obtaining torsional frequencies. Piezoceramic material G-1195 from Piezo Electric Products was selected because of its higher piezoelectric mechanical coupling effectiveness.[25] The piezo devices were placed at locations of high local strains natural with the beam modes. For cantilever beams, the clamped end is the location of high bending strain for the first two modes. Hence, two pairs of piezoceramic actuators, one pair each for flap and torsion modes, were placed near the clamped end. These devices were driven by sinusoidal signals with a maximum amplitude of 150 V, and the phase difference between the signals to the elements on opposite surfaces of a pair is 180 deg. Using special instrumentation, electric signals of different amplitude and phase at a frequency were generated to excite piezo devices at different stations.

Strain gauges were used to measure the response of rotating beams. In order to increase the signal-to-noise ratio, full bridges consisting of four active strain gauges for flap and torsion response were used. These bridges were bonded at different spanwise locations to measure mode shapes. Four strain gauges, bonded on two piezoceramic elements of the flap pair provide the induced strain signal which was used as an input function for frequency-response analysis. Frequency sweep of the excitation signal was carried out and fast Fourier transform (FFT) of the output signal with respect to the input signal was obtained using a spectrum analyzer. Thus, frequencies and amplitudes at resonances were obtained. A four-channel spectrum analyzer from Zonic was used to carry out the signal analyses of various bending and torsion strain gauge signals. To check the repeatability of the results, vibration tests were repeated two or three times. The beams were excited at the natural frequencies and respective strain modes were measured using strain gauges.

Results and Discussion

Free-vibration characteristics of bending-torsion coupled composite I-beams are presented, keeping in view the important features of open-section composite beam theory, i.e., constrained warping and lamination parameters of flanges and web. Table 1 shows the details of graphite-epoxy and Kevlar-epoxy I-beams examined in the present study. These beam configurations were selected so that the influence of warping constraints, fiber orientation, and rotational speed on natural frequencies could be studied.

Experimental Correlation

Figure 2 shows the frequencies and mode shapes of graphite-epoxy 15-deg I-beam of slenderness ratio 30 (IB1) with constrained warping effects included. Figure 3 shows similar results where constrained warping effects are not included. A shift of mode shape is noticed by comparing these figures. For example, with warping constraints included, the first mode corresponds to first lag-bending mode, the second mode refers

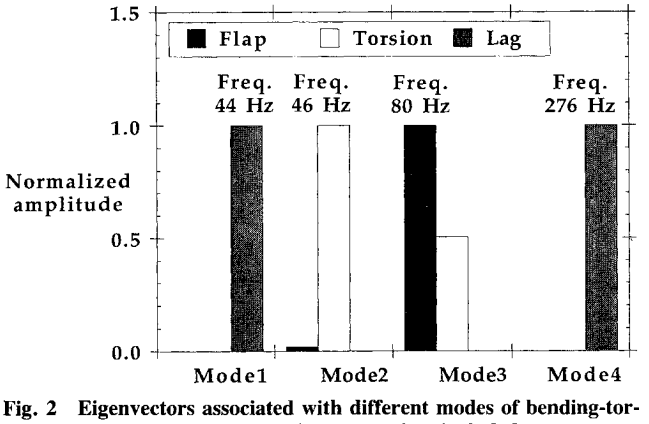

Fig. 2 Eigenvectors associated with different modes of bending-torsion coupled I-beam (IB1)-warping constraints included.

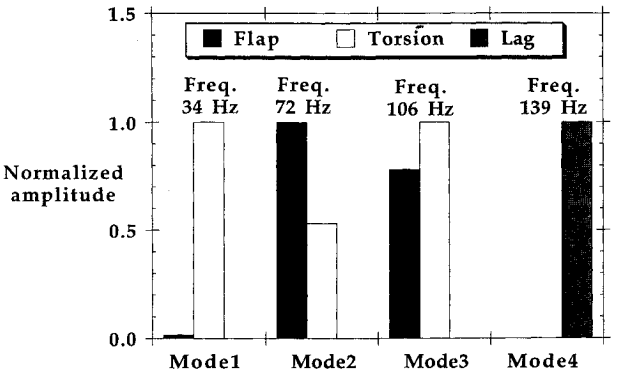

Fig. 3 Eigenvectors associated with different modes of bending-torsion coupled I-beam (IB1)-warping constraints not included.

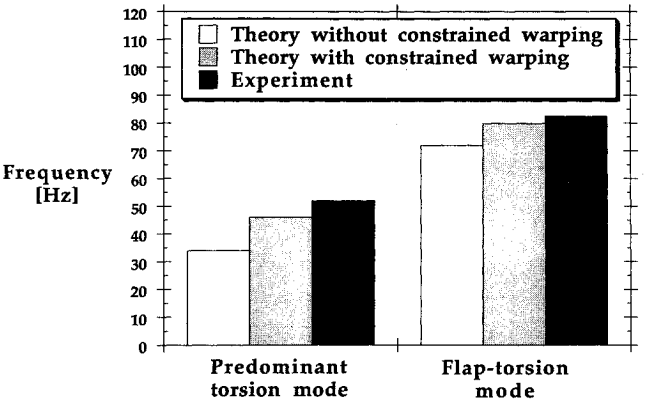

Fig. 4 Frequencies of bending-torsion coupled I-beam (IB1) of slenderness ratio 30.

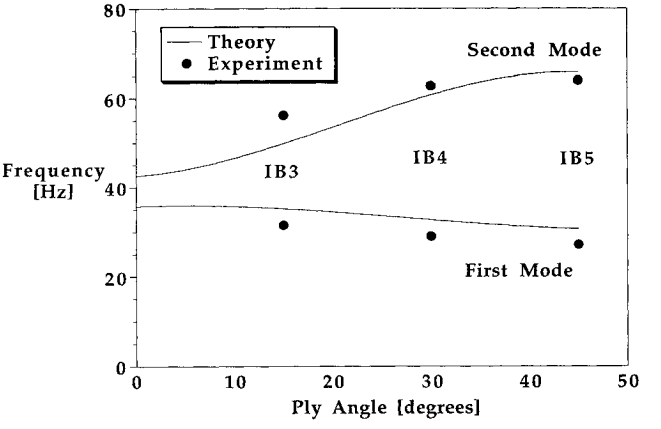

Fig. 5 Analytical and experimental frequencies of bending-torsion coupled graphite-epoxy I-beams.

to predominant torsion mode, the third mode is flap-torsion mode, and the fourth mode is second lag-bending mode. Without warping constraints, the first mode becomes predominant torsion, the second and third correspond to flap-torsion modes, and the fourth mode becomes lag bending mode. Figure 4 shows the comparison of experimental and theoretical frequencies of this beam corresponding to the first two modes. Because of inadequate force with piezoactuation, it was difficult to excite higher modes. Good correlation between experiment and theory with warping constraints is seen in this figure. μ for this beam is 1.62. Note that the warping constraints increase this frequency by about 35%.

Figure 5 shows the variation of natural frequencies with ply angle of last two layers of graphite-epoxy I-beams. It is important to note that the first frequency decreases with ply angle, whereas the second frequency increases with ply angle.

This is due to the fact that the first mode, being predominantly a bending mode, depends upon the bending stiffness which decreases with ply angle. However, the second mode, being predominantly a torsion mode, depends upon torsional stiffness which increases with ply angle. The correlation between theoretical and experimental frequencies corresponding to the first two modes (flap-torsion) of these beams is within 12%. Figure 6 shows similar results for Kevlar-epoxy beams. Good correlation between theory and experiment for fundamental frequencies of 15, 30, and 45 I-beams is noticed. The correlation between theoretical and experimental frequencies corresponding to the second mode is within 12%.

Figure 7 shows the influence of rotational speed on the fundamental frequency of Kevlar-epoxy 45-deg I-beam (IB9).

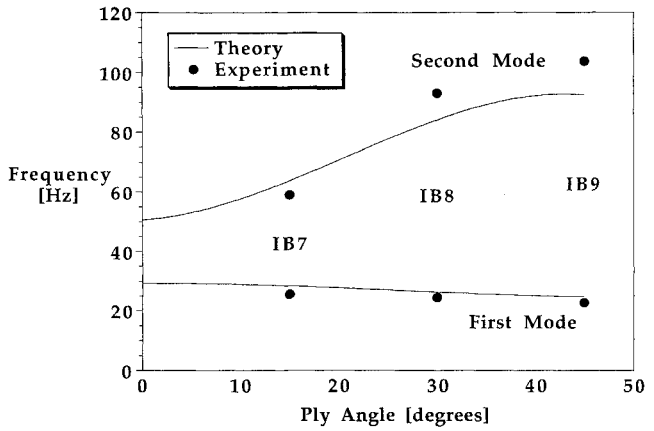

Fig. 6 Analytical and experimental frequencies of bending-torsion coupled Kevlar-epoxy I-beams.

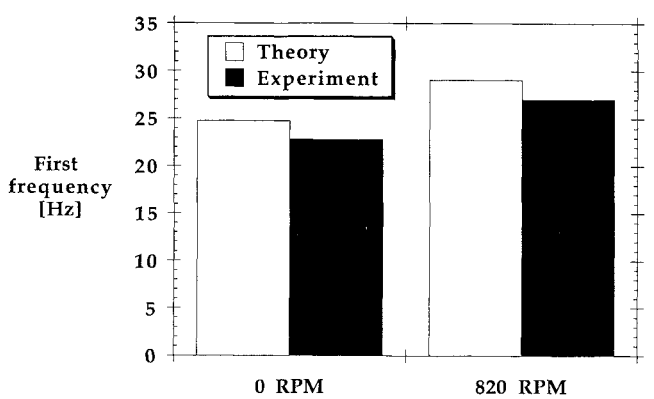

Fig. 7 Influence of rotational speed on first frequency of composite I-beam.

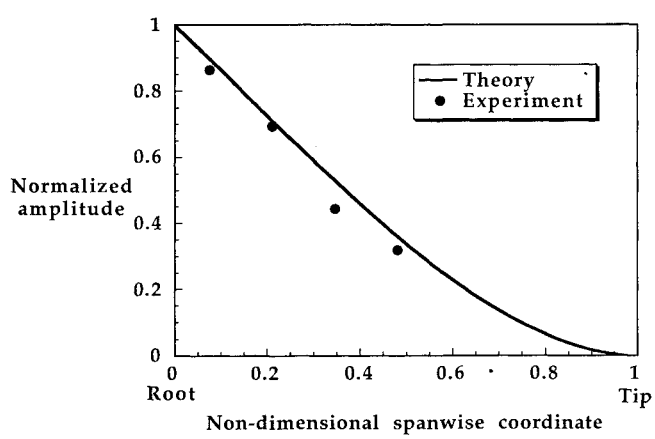

Fig. 8 Strain mode shape of composite I-beam.

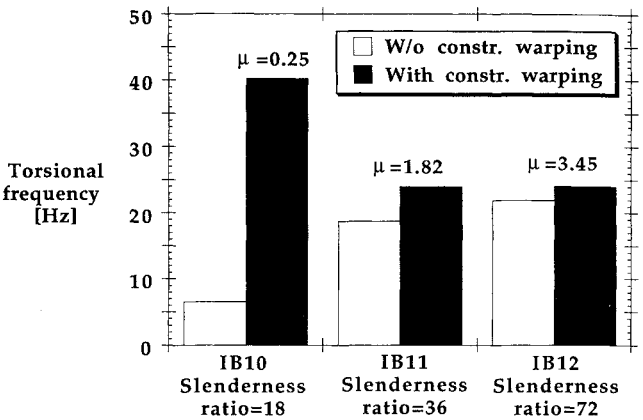

Fig. 9 Influence of constrained warping on torsional frequencies of composite I-beams.

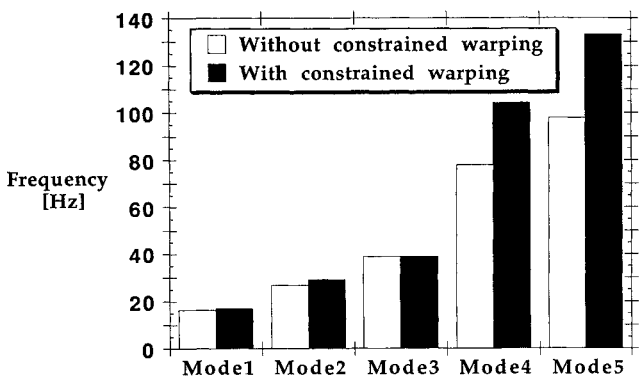

Fig. 10 Influence of constrained warping on frequencies of bending-torsion coupled I-beams (IB13).

The increase in this frequency at a rotational speed of 820 rpm is about 17%. The correlation between theory and experiment for nonrotating and rotating frequencies of this beam is within 10%.

Figure 8 shows the theoretical and experimental mode shapes in terms of bending strain for nonrotating graphite-epoxy I-beam (IB2). Good correlation between theory and experiment is seen from this figure.

Numerical Parametric Study

Figure 9 shows the influence of constrained warping on torsional frequencies of graphite-epoxy I-beams of different slenderness ratios. The slenderness ratio is defined as the ratio of length-to-height. Constraining the warping deformations increases the torsional stiffness of I-beam and this increase is inversely proportional to μ, which in turn depends upon the various cross-sectional stiffnesses and length of the beam.[22] The free-vibration characteristics of I-beam are influenced by constrained warping via an increase in torsional stiffness. Hence, the increase in frequency due to constrained warping is inversely proportional to the value of μ. For a beam with slenderness ratio of 18 (μ = 0.25), the increase in torsional frequency due to constrained warping effects is about 600%, whereas this increase for a beam with slenderness ratio of 36 is about 125%. A 10% increase is noticed for the beam with slenderness ratio of 72 (μ = 3.45). Thus, it is inferred that for beams with constrained warping parameter beyond 3.45, the torsional frequency is controlled by St. Venant torsion.

Figure 10 represents the constrained warping effects on natural frequencies of a bending-torsion coupled graphite-epoxy I-beam (IB13). Again, constrained warping increases the natural frequencies of torsion-related modes via an increase in torsional stiffness; the amount of increase being more at higher modes. This beam has bending-torsion cou-

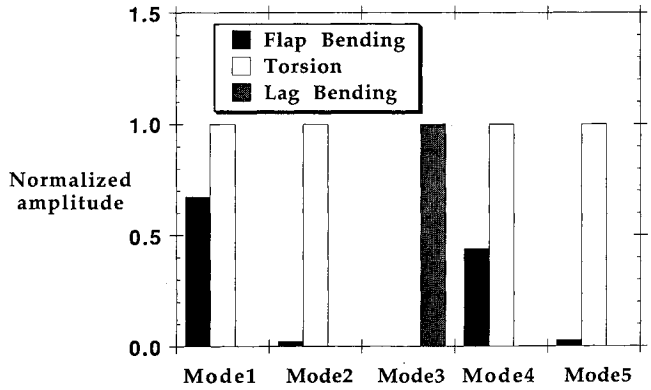

Fig. 11 Eigenvectors associated with different modes of bending-torsion coupled I-beam (IB13).

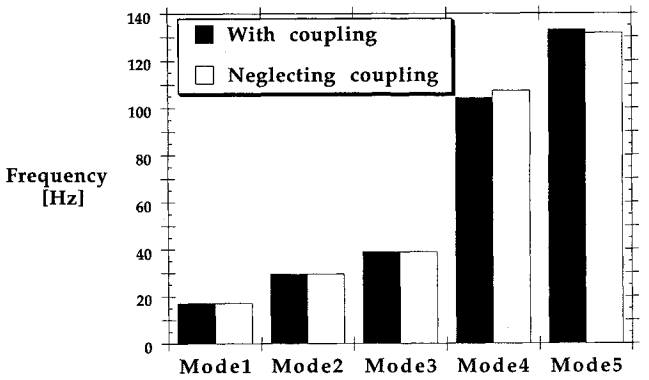

Fig. 12 Influence of bending-torsion coupling on natural frequencies of bending-torsion coupled I-beam (IB13).

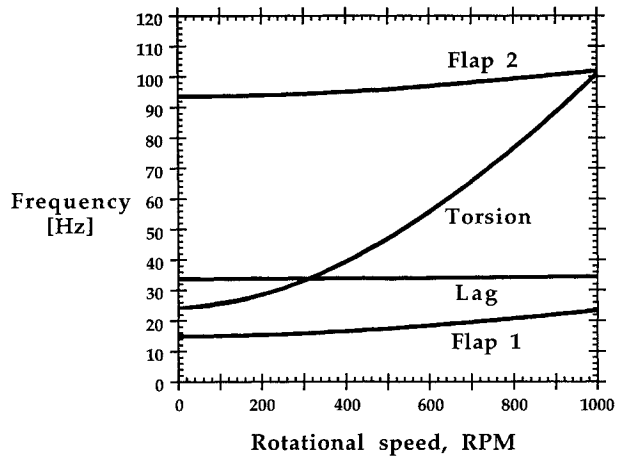

Fig. 13 Influence of rotational speed on natural frequencies of graphite-epoxy I-beam (IB12).

pling in the flapwise direction (normal to flange) but no coupling in the chordwise direction as the web has no angle plies. Figure 11 shows the relative tip amplitudes (eigenvectors) associated with different modes of this beam. Examination of eigenvectors reveals that first and fourth modes are strongly coupled. However, the second and fifth modes refer to predominantly torsion motion. Mode 3 refers to uncoupled lag-bending motion.

Figure 12 shows the influence of bending-torsion coupling on the natural frequencies of a bending-torsion coupled I-beam (IB13). These results include constrained warping. Note that the bending-torsion coupling changes the mode shapes. For example, the strongly coupled flap-torsion modes (modes 1 and 4 as shown in Fig. 11) will become uncoupled in the absence of coupling. However, the first five frequencies in both situations remain virtually unaltered. It is important to note that the bending-torsion coupling has a significant influence on coupling the modes, but only a slight influence on their natural frequencies.

Figure 13 shows the influence of rotational speed on natural frequencies for a graphite-epoxy I-beam (IB12). It is interesting to note that the increase in frequency because of rotational speed is higher for the torsional mode than for the flap or lag modes. This is as a result of stiffening due to centrifugal force (propeller moment effect). The increase in frequency corresponding to the first flap mode at a rotational speed of 1000 rpm is about 60%, whereas this increase corresponding to the first torsion mode is about 420%. The first lag and second flap frequencies do not change much with rotational speed.

Conclusion

Free-vibration analysis of rotating I-beams made out of general composite laminates is performed using Vlasov theory. The coupled flap-lag-torsion equations are solved using Galerkin's method. In order to provide experimental correlation to the theory, graphite-epoxy and Kevlar-epoxy I-beams of different fiber orientations were fabricated using an autoclave molding technique. These beams were tested for their vibration characteristics using an in vacuo rotor test facility. Based on this study, the following conclusions are drawn:

1) Constrained warping influences the natural frequencies of I-beams by increasing the torsional stiffness. The amount of increase is controlled by μ; the smaller the value of μ, the larger the effect of constrained warping. A typical increase of about 600% is noticed for the first torsional frequency of a graphite-epoxy 0/90 I-beam with μ equal to 0.25.

2) Bending-torsion coupling creates coupled flap-torsion modes for composite I-beams. It reduces the natural frequencies, with the amount of reduction controlled by the lay-up of the beams.

3) Rotational speed increases the natural frequencies of I-beams. For the beams considered in this study, the amount of increase is more in torsional modes than in flap and lag modes. The lag mode is least influenced by rotational speed.

Appendix: Elements of Matrices [P], [Q], [R], and [I_1]–[I_6]

$$P_{ij} = 0, \quad i \neq j \qquad P_{ii} = \lambda_i^4$$

$$Q_{ij} = 0, \quad i \neq j \qquad Q_{ii} = (2i - 1)^2$$

$$R_{ij} = 0, \quad i \neq j \qquad R_{ii} = (2i - 1)^4$$

$$I_{ij} = 0, \quad i \neq j \qquad I_{ii} = 1$$

$$I_{1ij} = \int_0^r (2i - 1)^3 \cos\left(\frac{2i - 1}{2}\frac{\pi z}{r}\right) \psi_j \, dx$$

$$I_{2ij} = \int_0^r (r^2 - z^2)\psi_{i,zz}\psi_j \, dz$$

$$I_{3ij} = \int_0^r z\psi_{i,z}\psi_j \, dz$$

$$I_{4ij} = \int_0^r \psi_{i,zzz} \sin\left(\frac{2j - 1}{2}\frac{\pi z}{r}\right) dz$$

$$I_{5ij} = \int_0^r \sin\left(\frac{2i - 1}{2}\frac{\pi z}{r}\right) \sin\left(\frac{2j - 1}{2}\frac{\pi z}{r}\right) \times (2i - 1)^2(r^2 - z^2) \, dz$$

$$I_{6ij} = \int_0^r \cos\left(\frac{2i - 1}{2}\frac{\pi z}{r}\right) \sin\left(\frac{2j - 1}{2}\frac{\pi z}{r}\right) (2i - 1)z \, dz$$

Acknowledgments

This research work has been supported by the Army Research Office under Contract DAAL-03-88-C-022, Technical Monitors, Robert Singleton and Tom Doligalski.

References

[1]Smith, E. C., and Chopra, I., "Formulation and Evaluation of an Analytical Model for Composite Box Beams," *Journal of the American Helicopter Society*, Vol. 36, No. 3, 1991, pp. 23–35.

[2]Rehfield, L. W., Atilgan, A. R., and Hodges, D. H., "Nonclassical Behavior of Thin-Walled Composite Beams with Closed Cross-Sections," *Journal of the American Helicopter Society*, Vol. 35, No. 2, 1990, pp. 42–51.

[3]Hodges, D. H., Atilgan, A. R., Fulton, M. V., and Rehfield, L. W., "Free Vibration Analysis of Composite Beams," *Journal of the American Helicopter Society*, Vol. 36, No. 3, 1991, pp. 36–47.

[4]Minguet, P., and Dugundji, J., "Experiments and Analysis for Composite Blades Under Large Deflections Part 1: Static Behavior," *AIAA Journal*, Vol. 28, No. 9, 1990, pp. 1573–1579.

[5]Stemple, A. D., and Lee, S. W., "Finite Element Model for Composite Beams with Arbitrary Cross Sectional Warping," *AIAA Journal*, Vol. 26, No. 12, 1988, pp. 1512–1520.

[6]Kosmatka, J. B., and Friedmann, P. P., "Vibration Analysis of Composite Turbopropellers Using a Nonlinear Beam-Type Finite-Element Approach," *AIAA Journal*, Vol. 27, No. 11, 1989, pp. 1606–1614.

[7]Bauchau, O. A., and Hong , C. H., "Large Displacement Analysis of Naturally Curved and Twisted Composite Beams," *AIAA Journal*, Vol. 25, No. 11, 1987, pp. 1469–1475.

[8]Chandra, R., Stemple, A. D., and Chopra, I., "Thin-Walled Composite Beams Under Bending, Torsional and Extensional Loads," *Journal of Aircraft*, Vol. 27, No. 7, 1990, pp. 619–627.

[9]Chandra, R., and Chopra, I., "Experimental-Theoretical Investigation of the Vibration Characteristics of Rotating Composite Box Beams," *Journal of Aircraft*, Vol. 29, No. 4, 1992, pp. 657–664.

[10]Nixon, M. W., "Extensional-Twist Coupling of Composite Circular Tubes with Application to Tilt Rotor Blade Design," *Proceedings of the 28th AIAA/ASME/ASCE/AHS/ASC Structures, Structural Dynamics and Materials Conference*, AIAA, Washington, DC, April 1989.

[11]Minguet, P., and Dugundji, J., "Experiments and Analysis for Composite Blades Under Large Deflections Part 2: Dynamic Behavior," *AIAA Journal*, Vol. 28, No. 9, 1990, pp. 1580–1588.

[12]Bauchau, O., Coffenberry, B. S., and Rehfield, L. W., "Composite Box Beam Analysis: Theory and Experiments," *Journal of Reinforced Plastics and Composites*, Vol. 6, No. 1, 1987, pp. 25–35.

[13]Atilgan, A. R., Hodges, D. H., and Fulton, M. V., "Nonlinear Deformation of Composite Beams: Unification of Cross-Sectional and Elastica Analyses," *Applied Mechanics Review*, Vol. 44, No. 11, Pt. 2, 1991.

[14]Hong, C. H., and Chopra, I., "Aeroelastic Stability of a Composite Blade," *Journal of the American Helicopter Society*, Vol. 30, No. 2, 1985, pp. 57–67.

[15]Hong, C. H., and Chopra, I.,"Aeroelastic Stability Analysis of a Composite Bearingless Rotor Blade," *Journal of the American Helicopter Society*, Vol. 31, No. 4, 1986, pp. 29–35.

[16]Panda, B., and Chopra, I.,"Dynamics of Composite Rotor Blades in Forward Flight," *Vertica*, Vol. 11, Nos. 1/2, 1987, pp. 187–209.

[17]Bousman, W. G., Ormistron, R. A., and Mirick, P. H., "Design Considerations for Bearingless Rotor Hubs," *Proceedings of the 39th Annual Forum of American Helicopter Society*, St. Louis, MO, May 9–11, 1983, pp. 509–536.

[18]Rehfield, L. W., and Atilgan, A. R., "On the Buckling Behavior of Thin Walled Laminated Composite Open Section Beams," *Proceedings of the 30th AIAA/ASME/ASCE/AHS/ASC Structures, Structural Dynamics and Materials Conference*, AIAA, Washington, DC, April 1989.

[19]Vlasov, V. Z., "Thin-Walled Elastic Beams," National Science Foundation and Dept. of Commerce (translated from Russian), USA, 1961.

[20]Gjelsvik, A., *The Theory of Thin-Walled Bars*, Wiley, New York, 1981.

[21]Bauld, N. R., Jr., and Tzeng, L. S., "A Vlasov Theory for Fiber Reinforced Beams with Thin-Walled Open Cross-Sections," *International Journal of Solids and Structures*, Vol. 20, No. 3, 1984, pp. 277–297.

[22]Chandra, R., and Chopra, I., "Experimental and Theoretical Analysis of Composite I-Beams with Elastic Couplings," *AIAA Journal*, Vol. 29, No. 12, 1991, pp. 2197–2206.

[23]Hodges, D. H., and Dowell, E. H., "Nonlinear Equations of Motion for the Elastic Bending and Torsion of Twisted Nonuniform Rotor Blades," NASA TN D7818, Dec. 1974.

[24]Lee, W. L., "Experimental Measurements of the Rotating Frequencies and Mode Shapes of a Full-Scale Helicopter Rotor in Vacuum," *Proceedings of the 35th Annual National Forum of the American Helicopter Society*, Washington, DC, May 1979.

[25]Crawley, E. F., and de Luis, J., "Use of Piezoelectric Actuators as Elements of Intelligent Structures," *AIAA Journal*, Vol. 25, No. 10, 1987, pp. 1373–1385.